The 2015 World Congress on
Advances in Structural Engineering and Mechanics (ASEM15)
Incheon, Korea, August 25-29, 2015

Interference between Two Tripped Cylinders in a Cross Flow

*Md. Mahbub Alam[1)]

[1)] *Institute for Turbulence-Noise-Vibration Interaction and Control, Shenzhen Graduate School, Harbin Institute of Technology, Shenzhen 518055, China*
[1)] *Key Kab of Advanced Manufacturing and Technology, Shenzhen Graduate School, Harbin Institute of Technology, Shenzhen 518055, China*
alamm28@yahoo.com

ABSTRACT

Flow interference is investigated between two tripped cylinders of identical diameter D at stagger angle α = 0° ~ 180° and gap spacing ratio P^* (= P/D) = 0.1 ~ 5, where P is the gap width between the cylinders and α is the angle between the freestream velocity and the line connecting the cylinder centers. Two tripwires, each of diameter 0.1D, were attached on each cylinder at azimuthal angle β = ±30°, respectively. Time-mean drag (C_D) and fluctuating drag (C_{Df}) and lift (C_{Lf}) on the two tripped cylinders were measured and compared with those on plain cylinders. Surface pressure measurements were also carried out to assimilate the fluid dynamics around the cylinders. C_D, C_{Df} and C_{Lf} all for the plain cylinders are strong function of α and P^* due to strong mutual interference between the cylinders, connected to six interactions, namely boundary layer and cylinder, shear-layer/wake and cylinder, shear layer and shear layer, vortex and cylinder, vortex and shear layer, and vortex and vortex interactions. C_D, C_{Df} and C_{Lf} are very large for vortex and cylinder, vortex and shear layer, and vortex and vortex interactions, i.e., the interactions where vortex is involved. On the other hand, the interference as well as the strong interactions involving vortex are suppressed for the tripped cylinders, resulting in insignificant variations in C_D, C_{Df} and C_{Lf} with α and P^*. In most of the (α, P^*) region, the suppressions in C_D, C_{Df} and C_{Lf} are about 58%, 65% and 85%, respectively, with maximum suppressions 60%, 80% and 90%.

Keywords: interactions; aerodynamics; two cylinders; tripped cylinders; trip wires; wake; forces; vortex; shear layer; staggered arrangement.

1. INTRODUCTION

[1)] Professor

In a real life architectural environment, most buildings and structures are in close proximity of each other, such as chimney stacks, tube bundles in heat exchangers, overhead power-line bundles, bridge piers, stays, masts, chemical-reaction towers, offshore platforms and adjacent skyscrapers. Fluid forces, Strouhal numbers (*St*) and flow structures are the major factors considered in the design of multiple slender structures subjected to cross flow. Alternate vortex shedding and vortex impingement may produce a large fluctuating pressure on the structures, causing structural vibrations, acoustic noise, and even resonance, which can trigger structural failure. Numerous failures in the practical applications of cylinder-like structures in cross flow have been illustrated in Chen (1987), Paidoussis (1981, 1993) and Blevins (1990). The cost associated with a typical engineering structural failure can easily reach the order of million dollars and even billions of dollars. Naturally, a concentrated effort is required to study and assimilate the fluid dynamics associated with multiple cylindrical structures in cross flow. Fluid-dynamic interference between two cylinders may give rise to flow separation, gap flow switching, shear-layer development, reattachment, vortex impingement, recirculation, quasi-periodic vortices and vortex street interaction, involving most of the generic flow features associated with multiple structures. Thus, flow around two cylinders provides an excellent model for gaining insight into the underlying flow physics around more structures

Depending on the interference effect between two cylinders, Zdravkovich (1988) and Mederios & Zdravkovich (1992) divided the whole region of possible arrangements of two cylinders into four regions. (i) *Proximity interference region*: the flow around either cylinder affects the other, occurring in both side-by-side and staggered cylinders at large α. The interference includes two wakes coupled each other, or narrow and wide wakes, and single combined wake. (ii) *Wake interference region*: it occurs in tandem and slightly staggered arrangements where the downstream cylinder influence on the upstream cylinder is insignificant, but the opposite is significant. It corresponds to coshedding flow. (iii) *Proximity and wake interference region*: in essence, it is the combination of the proximity and wake interference, occurring in tandem and staggered arrangements for small P^* and α at which the near wake of the upstream cylinder is disrupted by the downstream cylinder. Gu and Sun (1999) classified the proximity and wake interference into wake interference, shear layer interference, and proximity interference. (iv) *No interference region*: the flow of the either cylinder does not affect the other. This classification is useful from the engineering design point of view, though providing little information on the flow structure around the cylinders.

Extensive investigations have been conducted on the wake of two staggered cylinders in light of measurements of velocity field or flow structure (e.g., Sumner et al. 2000; Alam et al. 2005), Strouhal number *St* (e.g., Kiya et al. 1980; Alam and Sakamoto 2005), time-averaged pressure coefficient C_P (e.g., Igarashi 1981; Sun et al. 1992; Alam et al. 2005), fluctuating (rms) pressure coefficient C_P' (e.g., Alam et al. 2005), time-averaged drag C_D (e.g., Price and Paidoussis 1984; Alam and Meyer 2011), fluctuating drag C_D' (e.g., Price and Paidoussis 1984; Alam and Meyer 2011), time-averaged lift C_L (e.g., Gu et al. 1993; Alam and Meyer 2011) and fluctuating lift C_L' (e.g., Alam et al. 2005; Alam and Meyer 2011). Detailed measurements of flow field, *St* and forces enabled classifications of flow prevailing for two staggered cylinders (e.g., Kiya et al. 1980; Sumner et al. 2000; Alam and Meyer 2011). At Reynolds number Re = 1.58×10^4 based on free-stream velocity U_∞ and *D*, Kiya et al. (1980) measured *St* in the wake of two staggered circular cylinders for spacing ratio P^* = 0 – 4 and α = 0 - 90º, where *P* is the gap distance between the two cylinders, and α is the angle between the oncoming flow direction and the line connecting the cylinder centres. Depending on whether *St* was greater than or less than an isolated single cylinder Strouhal number St_0, they divided the P^*-α plane into five regions (region 1, $St > St_0$; region 2, $St < St_0$; region 3, bistable flow; region 4, single-body flow; region 4, weak or no vortex shedding; see Kiya et al. 1980 for the details of the regions).

With a very detailed measurement of C_D, C_D', C_L, C_L' and *St*, Alam and Meyer (2011) observed that C_D, C_L, C_D', C_L' and *St* are highly sensitive to P* and α, and simply flow classification based on interference are not enough to explain the variations in C_D, C_L, C_D', C_L' and *St*. Alam and Meyer (2011) therefore classified the whole α and P^* region based on individual cylinders and identified 19 distinct flow regimes. Each of them had different influences on the forces and *St*. There were two island-like regimes (α = 10° ~ 25°, P^*= 2.2 ~ 4.0; α = 18° ~ 32°, P^*= 2.1 ~ 5) where the values of C_{Df} and C_{Lf} were extensively high, about 2.35 and 1.58 times the single cylinder values. Maximum C_D of 1.75 acts on the cylinders in the regime of α = 90°, P^*= 2.2 ~ 2.6, which is about 1.56 times the single cylinder value. The information suggests that finding a flow control technique to reduce forces is necessary.

The use of spanswise tripping wires to trip the boundary layer is very interesting, bringing about a delayed separation, weaker shedding, and hence a reduction in forces. Previous researches showed that *St* and C_D characteristics strongly depend on the wire size, wire location and *Re* (e.g., James and Truong 1972; Nebres and Batill 1993; Aydin et al. 2014). James and Truong (1972) at $Re = 10^4 \sim 10^5$ investigated experimentally the dependence of a cylinder wake on the tripwire diameter (0.006 ~ 0.063*D)* and position β = 0° to 180°, where β is the angular position of a tripwire measured from the forward stagnation point. They found that a larger tripwire diameter results in the transition of the boundary layer to turbulence occurring at an earlier *Re* and/or a smaller β. Nebres and Batill (1993) studied the effect of a single wire of diameter 0.007*D* ~ 0.14*D* on the pressure distribution, *St* and C_D at *Re* = 2×10^4 ~ 4×10^4 and β = 0° ~ 180°. The tripwire had a considerable effect on the wake at β = 20° ~ 70° where a small change in β leads to large variation in both *St* and C_D. On the other hand, the tripwire had no effect on the wake when positioned near the forward stagnation point (β < 20°) or the base region.

Alam et al. (2003a) used tripwires with a diameter of 0.081*D* ~ 0.13*D.* The angular position of the tripping wire was varied from 20° to 60°. The optimum angular position of tripping rods for suppressing fluid forces was found to be 30° with C_D, C_{Df} and C_{Lf} were suppressed by 67%, 61% and 87%, respectively. Alam et al. (2010) conducted an experimental investigation in the wake of a circular cylinder with two tripwires (each of diameter 0.045*D*) attached at β = ±10° ~ ±70° at *Re* = 2.5×10^3 ~ 6×10^4. They identified five flow regimes based on forces, *St* and flow structure in the wake. Placing one tripwire of diameter varying from 0.029*D* to 0.059*D* at *Re* =5×10^3 ~ 3×10^4, Aydin et al. (2014) observed two critical locations of the wire where Karman instability attenuates and amplified, respectively.

While two staggered cylinders interact strongly each other and amplify forces, no methods have been developed to reduce forces or to weaken the interaction between them. The objective of this study is to reduce forces and interference between two staggered cylinders. Two tripwires are used on each cylinder at β = ±30° that is the optimum position obtained for a single isolated cylinder by Alam et al. (2003a). C_D, C_{Df} and C_{Lf} are measured for both cylinders with α varying from 0° to 180° and P^* from 0.1 and 5.0. The measured forces on the tripped cylinders are compared with those on plain cylinders and reductions of forces are estimated. Pressure measurements are also conducted for both plain and tripped cylinders.

2. EXPERIMENTAL DETAILS

Experiments were done in a closed-circuit wind tunnel with a 2.5-m-long rectangular test section of 1.20×0.30 m at the fluid mechanics laboratory of Kitami Institute of Technology, Japan. See Alam et al. (2005) for the details of the wind tunnel. The cylinders spanned the horizontal 0.3-m dimension of the tunnel. In the test section side walls, two circular holes of 0.5 m diameter, one opposite to the other, were made where two circular disks, each included a slit for cylinders, marked 0° - 360° with a resolution of 1°, were placed (Fig. 1c). The disks were rotatable to adjust the stagger angle α (Fig. 1a). Two circular cylinders of a diameter D = 49 mm, made of brass, spanned horizontally the 0.3-m dimension. The free-stream velocity, U_∞, was 17 m/s, resulting in Re ($\equiv U_\infty D/\nu$) = 5.5 × 10^4, where ν is the kinematic viscosity of air. In order to check the spanwise uniformity of flow as well as spanwise separation of flow over a single cylinder for fluid forces being measured by a load cell (which will be discussed next), circumferential time-averaged and fluctuating pressures on the surface of the cylinder at the mid-section, and at ±35mm and ±80mm (from the mid-section), were measured. The results showed that the time-averaged and fluctuating pressure distributions at the five different sections were the same within the accuracy of measurement. The geometric blockage ratio was 4% based on single cylinder; total blockage for the cylinder pair was 8%. Based on their measurements, West and Apelt (1982) suggested that the blockage had virtually no effect on forces if less than 6% and could have a very small effect if between 6% and 9%. Therefore, the present blockage (8%) is expected to have a negligible effect on C_D. The cylinder aspect ratio at the test section was 6.1. West and Apelt (1993) established that the forces on an elemental section are independent of spanwise location for aspect ratios greater than 10, i.e., ‘long’ cylinder conditions occur. From the result published by Szepessy and Bearman (1992), it was found that the force was about 3% higher for an aspect ratio of 6 than that for the aspect ratio of 10. More details of the tunnel and blockage and aspect ratio effects can be found in Alam et al. (2003b, 2005).

Figure 1(b) shows a symmetrical arrangement of two tripping rods, each 5-mm diameter, on a cylinder and the coordinate system. β is the angular position of a tripping wire (Fig. 1b) and θ is the azimuthal angle measured from the nominal front stagnation point (Fig. 1a). As fluid forces were measured using load cell, a gap between a tripping wire and the cylinder was required. To understand the influence of the gap on forces, the gap ratio was varied from δ/D = 0.008 to 0.22 (δ = 0.4 ~ 12 mm) and it was found that fluid force coefficients all were almost independent of the gap ratio for δ/D < 0.15. See Alam et al. (2003a) for more details.

Two pairs of square blocks, as shown in Fig. 1(d), were used to hold the tripping wires and the cylinder to the tunnel wall. Each block has two holes at β = ±30° with δ/D = 0.008 mm, where the tripping wires were placed precisely. The diameters of the holes for the tripping wires were the same as the diameters of the tripping wires, and each hole was 35 mm in length. As a result, fluid forces acting on the tripping wires did not cause any vibration or rotation of the tripping rods.

Fluid forces were measured over a small spanwise length of the cylinders, using load cells (Fig. 1e). The cylinder to be measured was built in with an active ('live') section of a spanwise 45 mm (0.92*D*) length and two dummy sections. This size was determined taking into account the cross-correlation length of fluctuating pressure in the spanwise direction of the cylinder. The active section, placed between the two dummy sections, corresponded to the midspan of the cylinder and was installed with a load cell that consisted of four semiconductor strain gauges.

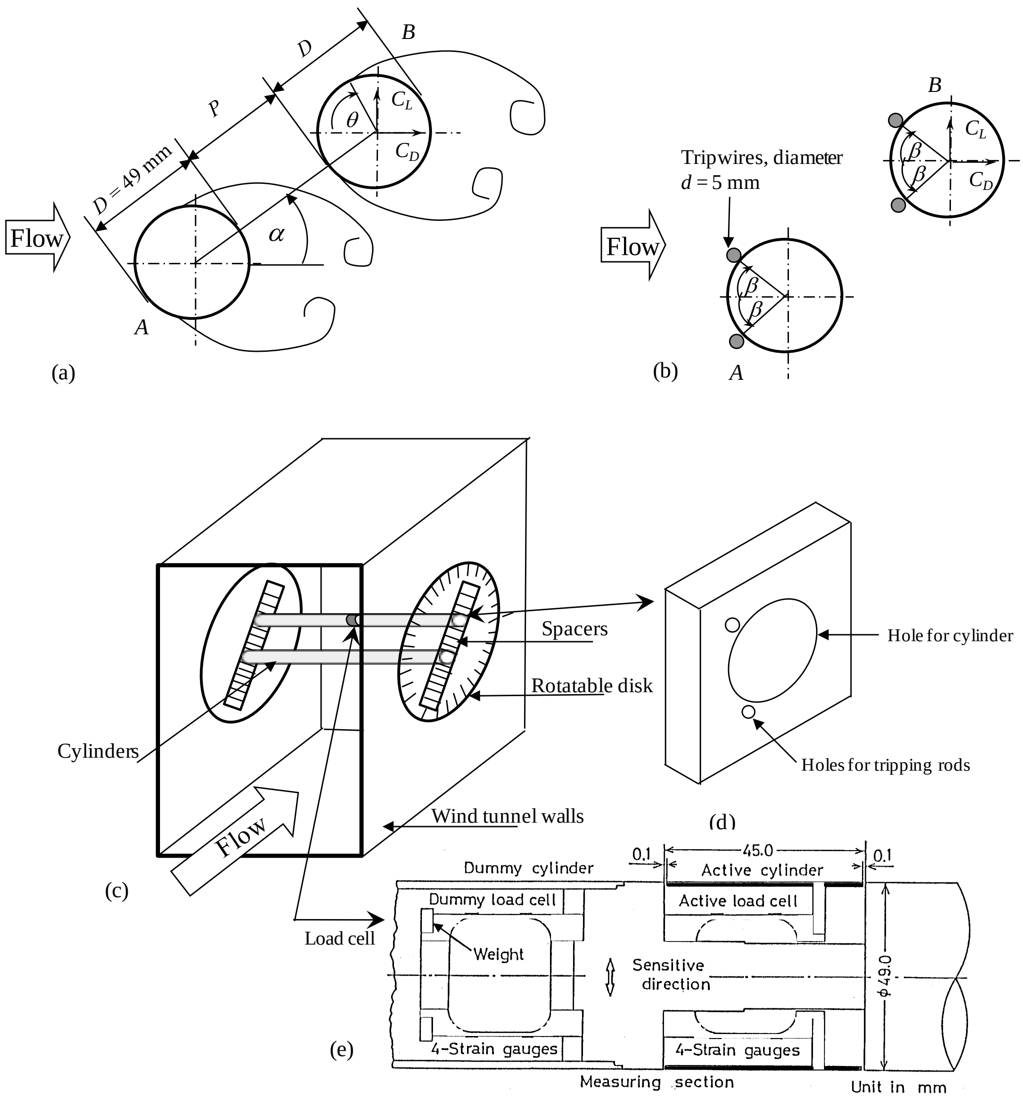

Fig. 1 Definitions of symbols and arrangement of cylinders: (a) plain cylinders, and (b) tripped cylinders. (c) A schematic of experimental setup, (d) block for holding cylinder and tripping wires, and (e) load cell details.

One of the dummy sections was also instrumented with another load cell of the same configuration. The load cell inside the active section measured a combination of fluid forces and forces due to vibration transmitted from outside through the cylinder support, whilst that inside the dummy section measured the latter forces only. Hence the fluid forces acting on the active section could be calculated by subtracting the output of the load cell inside the dummy section from that of the load cell inside the active section. The sensitivity of the load cells was 11.311 mV/g. See Sakamoto et al. (1994) or Alam et al. (2005) for the load details.

A semiconductor pressure transducer (Toyoda PD104K) with a range of ±10 kPa was used to measure the surface pressure during experiments. The transducer output was calibrated to give a reading of 6.22 V for 1 kPa of applied pressure. The pressure transducer responded to pressure fluctuation up to 500 Hz with a gain factor of 1±0.06, the phase lag being negligible.

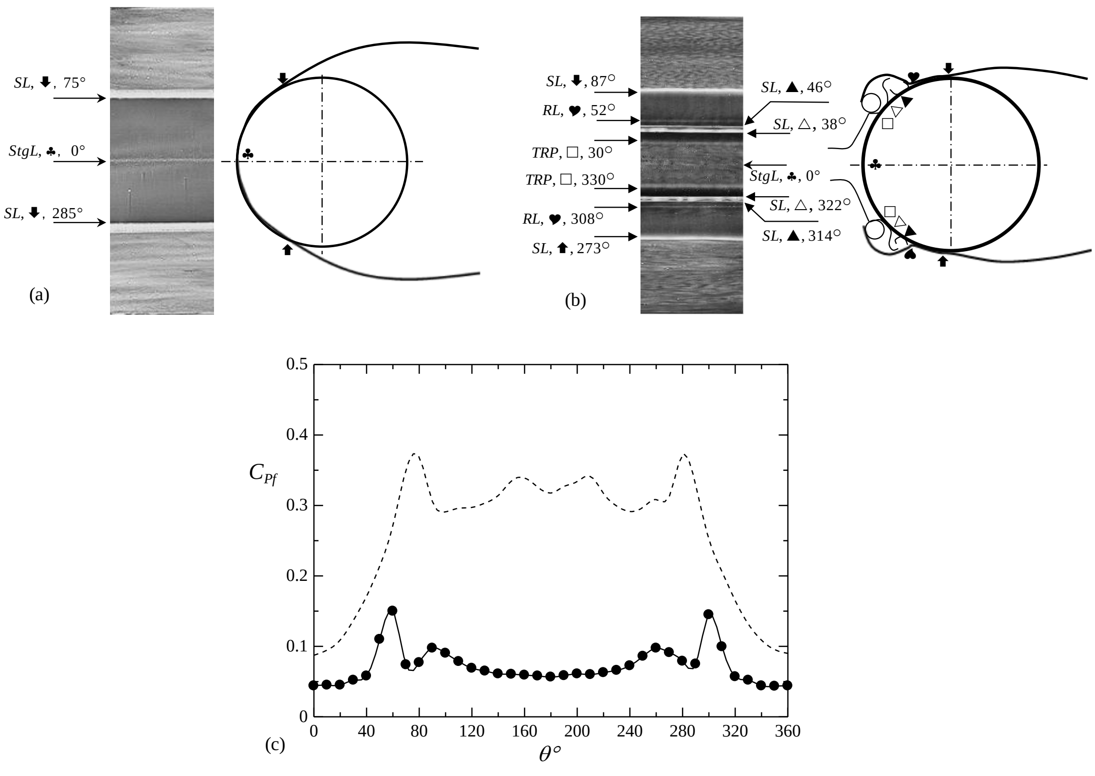

Fig. 2 Oil-flow patterns and corresponding sketch of flow for (a) single plain cylinder, and (b) single tripped cylinder: *TRP*, tripping wire position; *RL*, reattachment line; *SL*, separation line; *StgL*, stagnation line. (c) Fluctuating pressure C_{Pf} distribution on the surface of a single cylinder: - - - -, plain cylinder; ●, tripped cylinder. Alam et al. (2003a).

3. FLOW AROUND A SINGLE CYLINDER WITH TRIPWIRES

Here we will provide an overall picture of the flow structures around a single isolated tripped cylinder. Here a tripped cylinder means the cylinder with tripwires. Fig. 2 shows surface oil-flow pattern, the corresponding flow sketch and fluctuating pressure C_{Pf} distribution on a tripped and a plain cylinder. For the plain cylinder, the boundary layers separate at about $\theta = 75°$ and 285° (Fig. 2a) corresponding to the maximum C_{Pf} in the distribution (Fig. 2c). On the other hand, the surface oil-flow pattern (Fig. 2b) shows that the two boundary layers separating from the tripping wires reattach on the cylinder surface behind the wires at $\theta = 52°$ and 308°, respectively. The reattachments are followed by laminar separations at $\theta = 87°$ and 273°. These reattachment and separation positions correspond to the sharp and small peaks, respectively, in C_{Pf} distribution (solid circle symbol). The magnitude of C_{Pf} on the whole surface is considerably smaller for the tripped cylinder than the plain cylinder, inferring that the alternating Karman type vortex is almost suppressed or very weak. For more details, refer to Alam et al. (2003a).

4. INTERACTION BETWEEN PLAIN CYLINDERS

Based on mechanisms of interactions between the cylinders, Alam and Meyer (2011) classified the whole region of $\alpha = 0° - 180°$ and $P^* = 0.0 - 5.0$ into six interaction regimes, namely boundary layer and cylinder interaction; shear-layer/wake and cylinder interaction; shear layer (SL) and shear layer (SL) interaction; vortex and cylinder interaction; vortex and shear layer (SL) interaction; and vortex and vortex interaction. The regimes of the interactions in P^*-α are shown in Fig. 3.

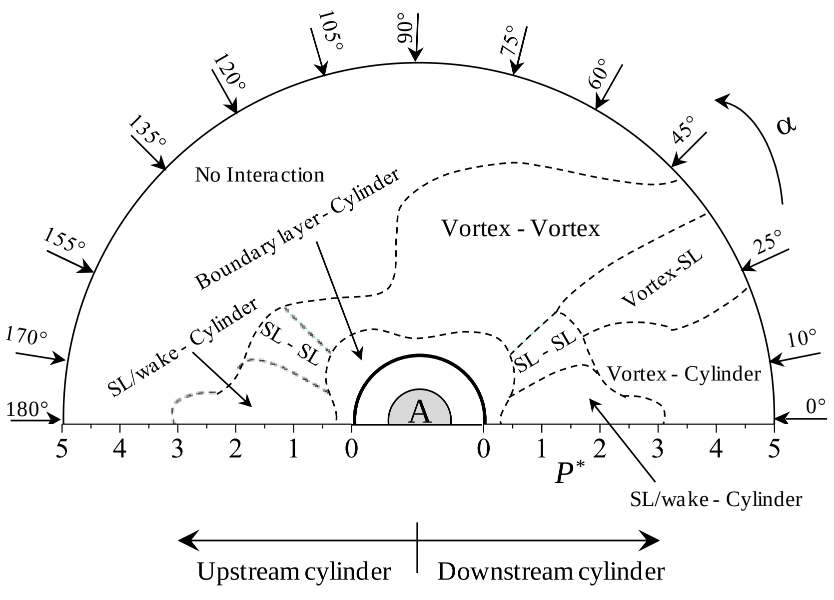

Fig. 3 Possible interactions and their regimes in P^* - α plane for plain cylinders. SL: shear layer.

For the purpose of simplicity, it can be described with reference to Fig. 1(a), in which the cylinder *A* is tentatively assumed to be fixed, and thus the two parameters P^* and α suffice to determine the arrangement of the two cylinders. It may be noted that the cylinder *B* is the downstream cylinder for $\alpha < 90°$ and it becomes the upstream cylinder for $\alpha > 90°$. At the peripheries of the inner and outer half-circles, the values of P^* are 0.0 and 5.0, respectively. How these interactions are connected to C_D, C_{Df} and C_{Lf} can be observed in contours of C_D, C_{Df} and C_{Lf} on a P^* - α plane shown in Figs. 4(a), 5(a) and 6(a). While vortex and cylinder, and vortex and shear layer interactions enhance C_{Df} and C_{Lf}, both shear-layer/wake and cylinder, and boundary-layer and cylinder interactions weaken C_{Df} and C_{Lf} (Figs. 3, 5a, 6a). Vortex and vortex interaction results in high C_D and C_{Lf} (Figs. 3, 4a, 6a). Shear layer and shear layer brought about the multiple frequencies in the wake (Alam and Meyer 2011). It is interesting from the above observation that C_D, C_{Df} and C_{Lf} are amplified for the interactions where vortex is involved. Thus, it is worth examining how C_D, C_{Df} and C_{Lf} behave when sheddings of vortices are suppressed or weakened using tripwires.

5. TRIPPED CYLINDERS

Figs. 4, 5 and 6 display a comparison of C_D, C_{Df} and C_{Lf} on a P^*- α plane between the plain and tripped cylinders. In the scale bars, the color or the range marked by '*' and '♠' indicates the value of a single isolated plain and tripped cylinders, respectively. As mentioned above, the left and right sides of a contour map show the values of coefficient of the upstream and downstream cylinders, respectively. Note that the values of C_D, C_{Df}, and C_{Lf} of a single plain cylinder are 1.12, 0.14, and 0.48, respectively and those of a single tripped cylinder are 0.38, 0.05 and 0.07.

5.1. Steady fluid force

For the case of plain cylinders, it is seen that the upstream cylinder experiences somewhat lower C_D at α = 120°-180°, $P^* < 3.0$ than a single isolated cylinder (Fig. 4a). The downstream cylinder experiences highly negative C_D at $\alpha < 10°$, $P^* < 3.0$, with a maximum negative value of -0.72 when it is in contact with the upstream cylinder at α = 0°. Both are connected to shear-layer/wake and cylinder interactions. Maximum C_D acts on the two cylinders at α = 90°, P^* = 1.2 ~ 2.0, where an enhanced antiphase vortex shedding occurs from the cylinders (Fig. 4c), associated with vortex and vortex interactions. A significantly higher C_D acts on the upstream cylinder at α = 90° ~ 120°, P^* < 0.2 due to formation of separation bubble (Alam et al. 2005) resulted from boundary layer and cylinder interaction. For the tripped cylinders (Fig. 4b), a significant reduction in C_D in comparison with the plain cylinders is observed over the whole region except at α = 90° ~ 120°, P^* < 0.2 that nestles in the boundary layer and cylinder interaction. The maximum C_D (α = 90°, P^*= 1.2 ~ 2.0) appearing in vortex and vortex interaction is suppressed for the tripped cylinders, by about 60%. The C_D on the most of the region for the plain cylinders is 1.04 ~ 1.26 (Fig. 4a) which have been suppressed to 0.38 ~ 0.6 for the tripped cylinders (Fig. 4b). On an average, the suppression in C_D is about 58%. Figure 4(b) indicates that mutual interference between the cylinders greatly weakens when the tripping wires are used on the cylinders. This is because now the sheddings from the two tripped cylinders is very weak.

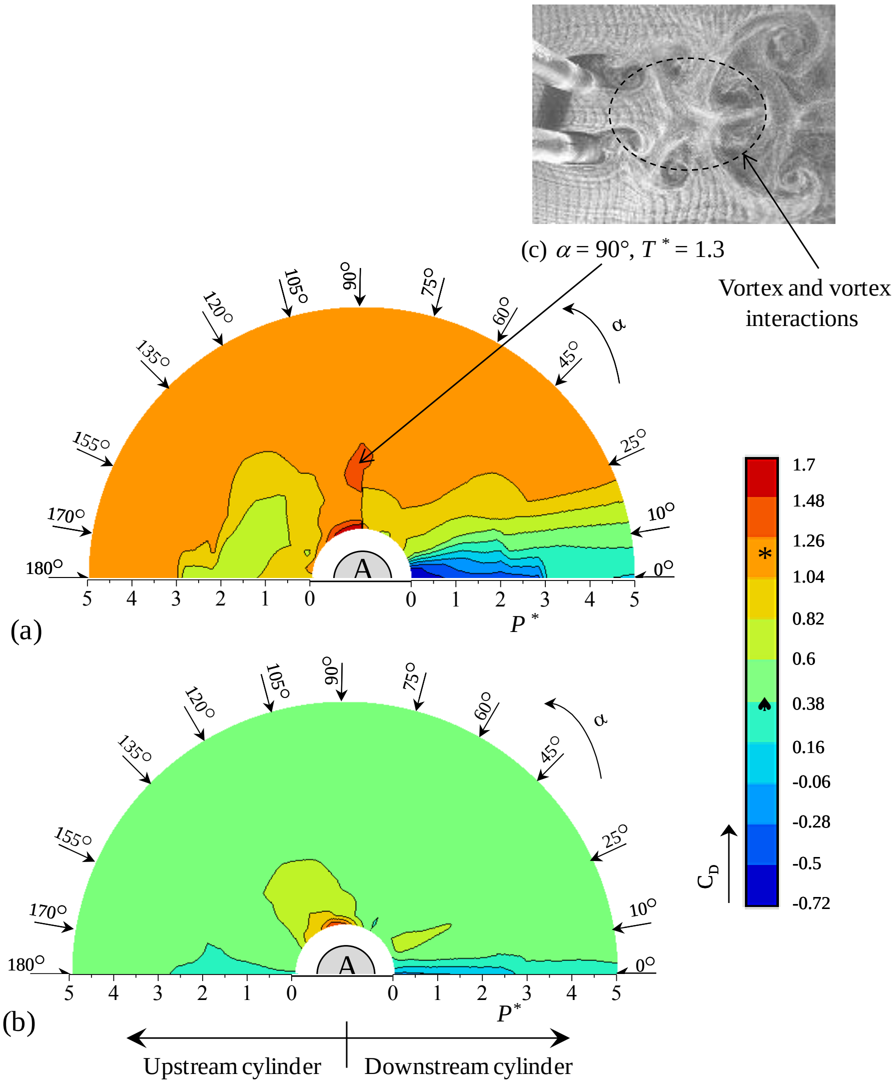

Fig. 4 Contour plot of time averaged drag coefficient, C_D: (a) plain cylinders (Alam and Meyer 2011), (b) tripped cylinders. '*' and '♠' denotes C_D values of a single cylinder plain and tripped, respectively. (c) The flow structure corresponding to the maximum C_D.

5.2. Fluctuating fluid force

For the case of plain cylinders, significantly higher magnitudes of C_{Df} and C_{Lf} act on the downstream cylinder at α = 5° ~ 25° (P^* > 2.5) and α = 15° ~ 35° (P^* > 2.5), respectively (Figs. 5a, 6a), connected to vortex and cylinder (Fig. 5c) and vortex and shear layer (Fig. 6c) interactions. The mechanisms of producing the maximum C_{Df} and C_{Lf} are different. The large magnitude of C_{Df} is caused by the alternate strike of the upstream cylinder vortices on the front surface of the downstream cylinder (Fig. 5c). On other hand, that of C_{Lf} results from the alternate vortices passing over the lower surface of the downstream cylinder (Fig. 6c). C_{Lf} and C_{Df} on the upstream cylinder become extremely small for α = 120° ~ 180°, P^* < 3.0 and on both cylinders in the vicinity of side-by-side arrangement at small P^*. In the former region, they become very small because formation of fully developed Karman vortex behind the upstream cylinder is retarded by the presence of the downstream cylinder (Alam et al. 2005). In the latter region, the gap flow between the cylinders acts as a base bleed, propelling the rolling positions of the outer shear layers downstream, causing small C_{Lf} and C_{Df}.

C_{Df} of the tripped cylinders is suppressed to very small value for the whole region, compared to that of the plain cylinders. The value of C_{Df} in the region α = 10° ~ 25°, P^* = 2.5 ~ 3.5 is maximum, 0.30 ~ 0.34, for the plain cylinders and 0.15 ~ 0.19 for the tripped cylinders. The reduction is indeed due to the absence of interaction between vortex and cylinder as the vortices are suppressed for the tripped cylinders. Here also the mutual interference between the tripped cylinders is very small. A dramatic decrease in C_{Lf} is self-evident for the tripped cylinders compared to the plain cylinders (Fig. 6b). C_{Lf} in the red region (maximum values of C_{Lf}) of the plain cylinders reduces to a significantly small value with the tripping wires added on the cylinders; the reduction is about 70%. Again while the large value of C_{Lf} is ascribed to the vortex and shear layer interaction in the plain cylinder case, C_{Lf} is small for tripped cylinders as there is no significant vortex and shear layer interaction. Thus the use of tripping wires on two cylinders is an effective means for suppressing interactions associated with vortex.

C_D, C_{Df} and C_{Lf} of the plain cylinders briskly vary with change in P^* and α (Figs. 4a, 5a, 6a) due to emergence of many flow features including shear layer reattachment, vortex impingement, triggering, vortex coupling, shear layer instability, etc, engendered by the six interactions (Alam and Meyer 2011). However, those of the tripped cylinders vary rather mildly. The observation suggests that interference between the plain cylinders is much strong but that between the tripped cylinders is very weak. For the case of tripped cylinders, the flow around the cylinders over the entire region is almost the same except $\alpha < 25°$. In other words, the mentioned features appearing for the plain cylinders are suppressed or their actions are insignificant for the tripped cylinders; mutual interference effect between the cylinders is reduced significantly; as a result, C_D, C_{Df} and C_{Lf} are almost insensitive to P^* and α.

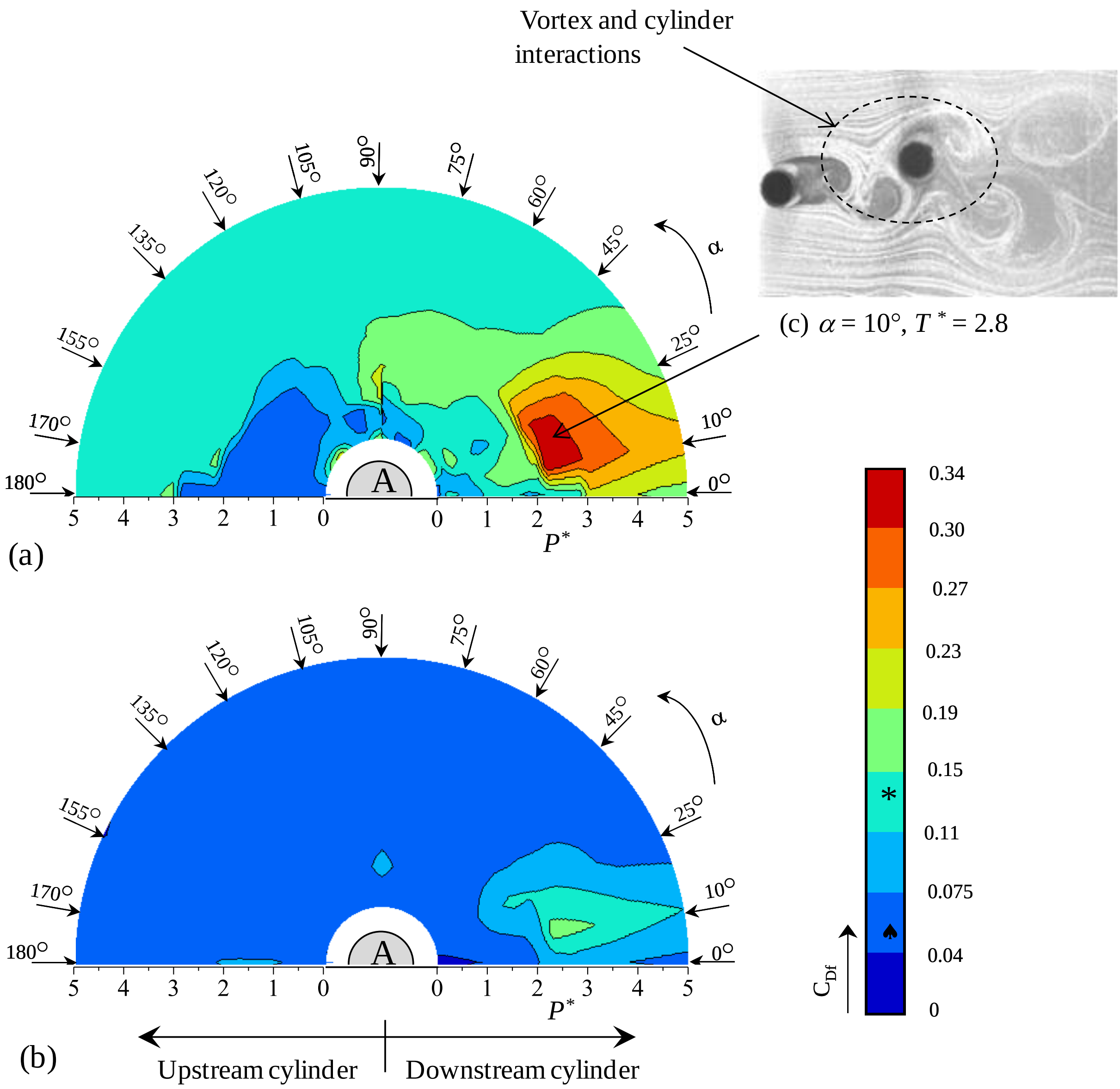

Fig. 5 Contour plot of fluctuating drag coefficient, C_{Df}: (a) plain cylinders (Alam and Meyer 2011), (b) tripped cylinders. '*' and '♠' denotes C_{Df} values of a single cylinder plain and tripped, respectively. (c) The flow structure corresponding to the maximum C_{Df}.

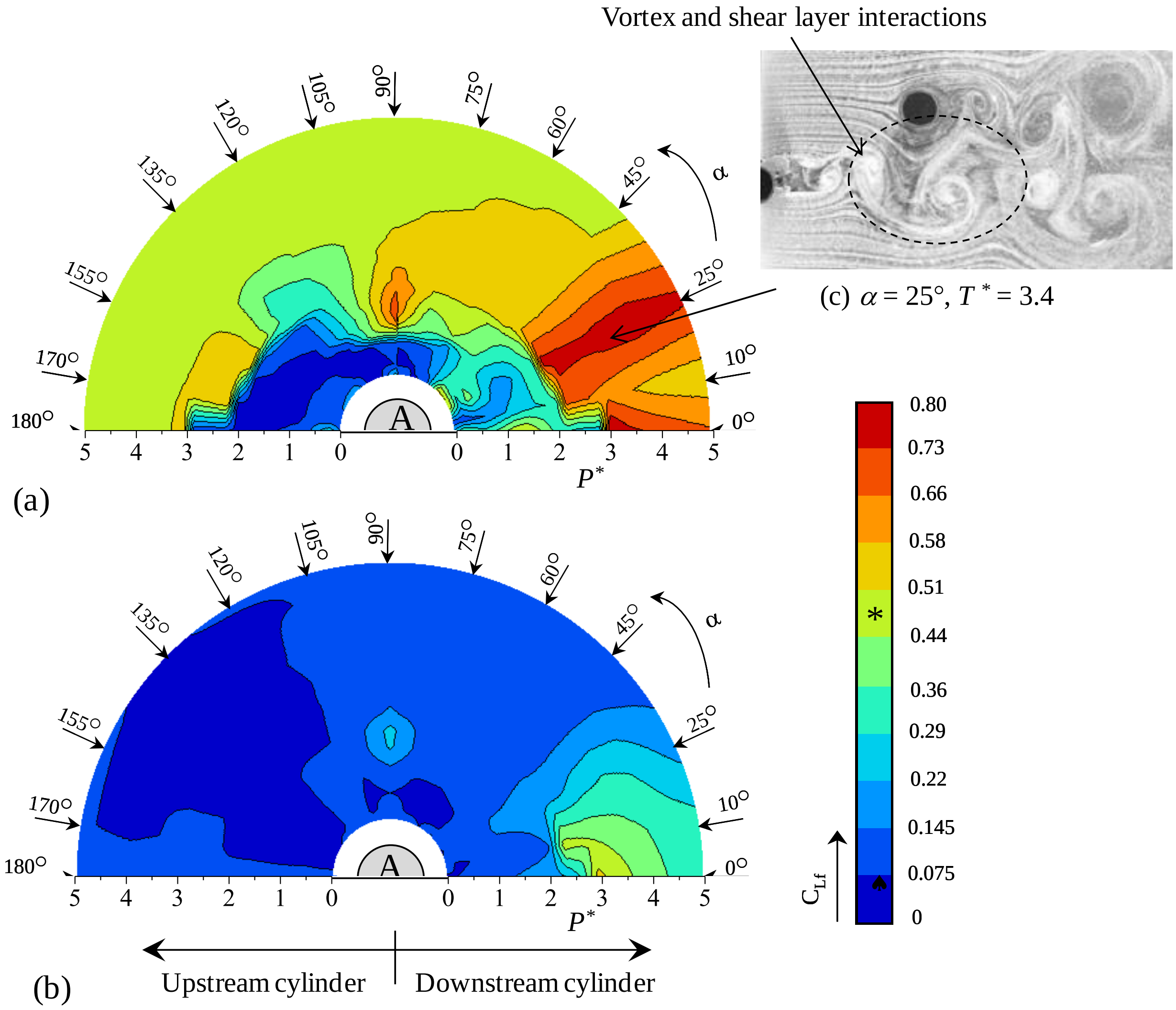

Fig. 6 Contour plot of fluctuating lift coefficient, C_{Lf}: (a) plain cylinders (Alam and Meyer 2011), (b) tripped cylinders. '∗' and '♠' denotes C_{Lf} values of a single cylinder plain and tripped, respectively. (c) The flow structure corresponding to the maximum C_{Lf}.

As sketched in Fig. 2(b), the flow structure on the tripped cylinders has the following features: (i) the shear layer separating from the tripwires reattaches on the cylinder surface, (ii) the eventual separation is postponed, (iii) wake narrows, and (iv) vortex shedding is almost suppressed from the cylinders. A cylinder with these features could not interfere the other. However, for α < 25°, the downstream cylinder is submerged in the wake of the upstream cylinder, hence interfered weakly.

5.3. Quantitative suppression

As seen in Figs. 5 and 6, quantitative magnitudes of suppression in C_{Df} and C_{Lf}

are not the same at all over the region, but dependent on P^* and α. For the plain cylinders, there are some regions where C_{Df} and C_{Lf} are very small, such as α =135° ~ 180°, P^* < 2. In these regions, considerable suppression in C_{Df} and C_{Lf} cannot be expected because values C_{Df} and C_{Lf} in those regions are already small. So it may also be an important point to quantify local suppressions in C_{Df} and C_{Lf}.

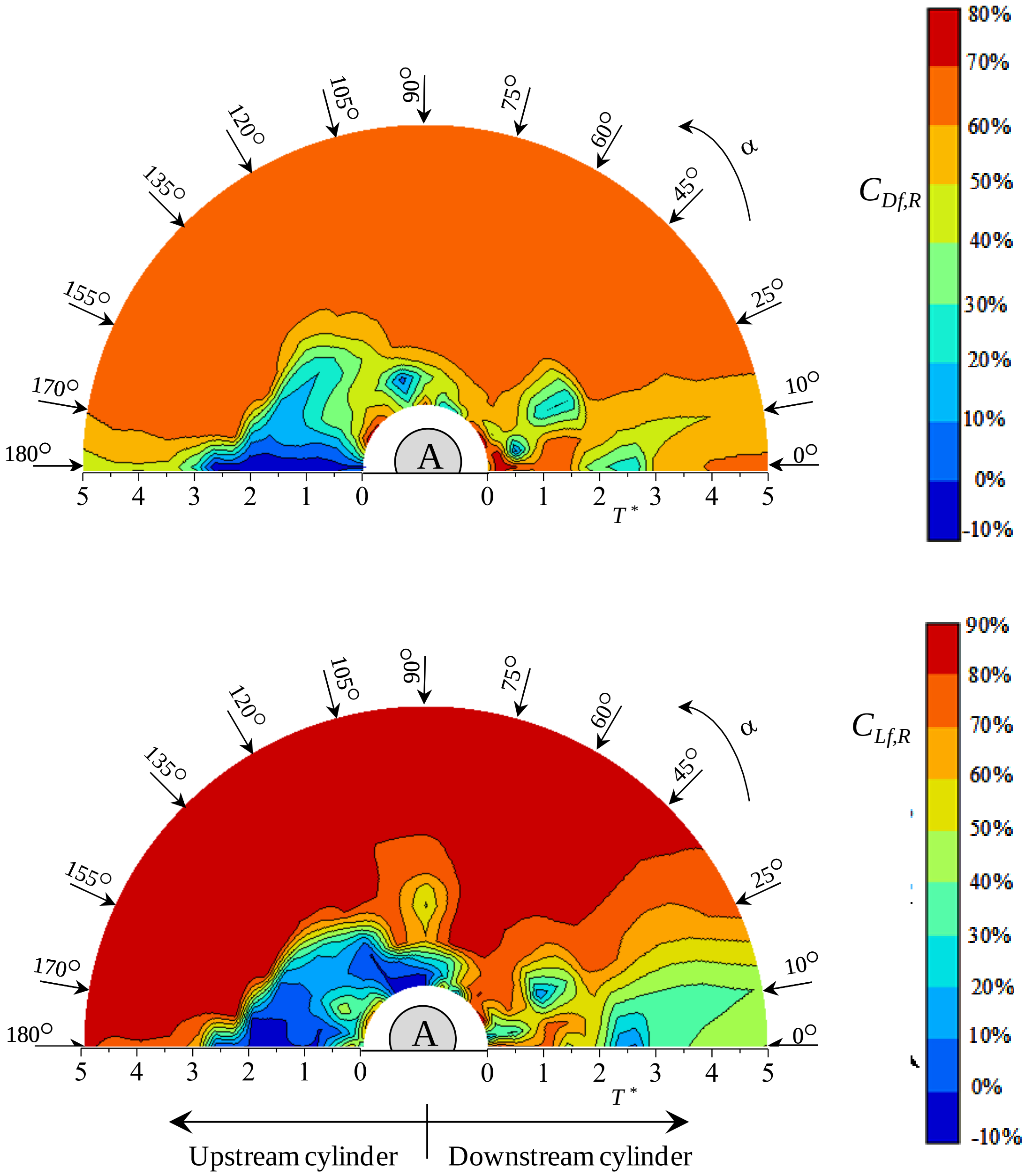

Fig. 7 Percent of local suppression in C_{Df} and C_{Lf} in α -P^*. (a) $C_{Df,R}$ and (b) $C_{Lf,R}$.

The local suppressions in C_{Df} or C_{Lf} can be estimated as,

%local suppression in C_{Df}, $C_{Df,R}(\alpha, P^*) = \dfrac{C_{Df,PC}(\alpha, P^*) - C_{Df,TC}(\alpha, P^*)}{C_{Df,PC}(\alpha, P^*)} \times 100$, and

%local suppression in C_{Lf}, $C_{Lf,R}(\alpha, P^*) = \dfrac{C_{Lf,PC}(\alpha, P^*) - C_{Lf,TC}(\alpha, P^*)}{C_{Lf,PC}(\alpha, P^*)} \times 100$,

where the suffices *PC* and *TC* refer to plain cylinders and tripped cylinders, respectively.

Local suppression in C_{Df} and C_{Lf} is presented in Fig. 7. Maximum values in the scale bar are presented as 80% and 90% for $C_{Df,R}$ and $C_{Lf,R}$, respectively; suppressions of the coefficients more than those were not occurred. It is clear from the figures that, in most of the region, C_{Df} and C_{Lf} are suppressed by about 65% and 85%, respectively. There are some regions where $C_{Df,R}$ and $C_{Lf,R}$ negative (0 ~ -10%). Negative suppression means the values of coefficient for the tripped cylinders are greater than those of the plain cylinders, i.e., C_{Df} and C_{Lf} are not suppressed by using tripping rods. Indeed, these are the regions where values of C_{Df} and C_{Lf} of the plain cylinder are very small.

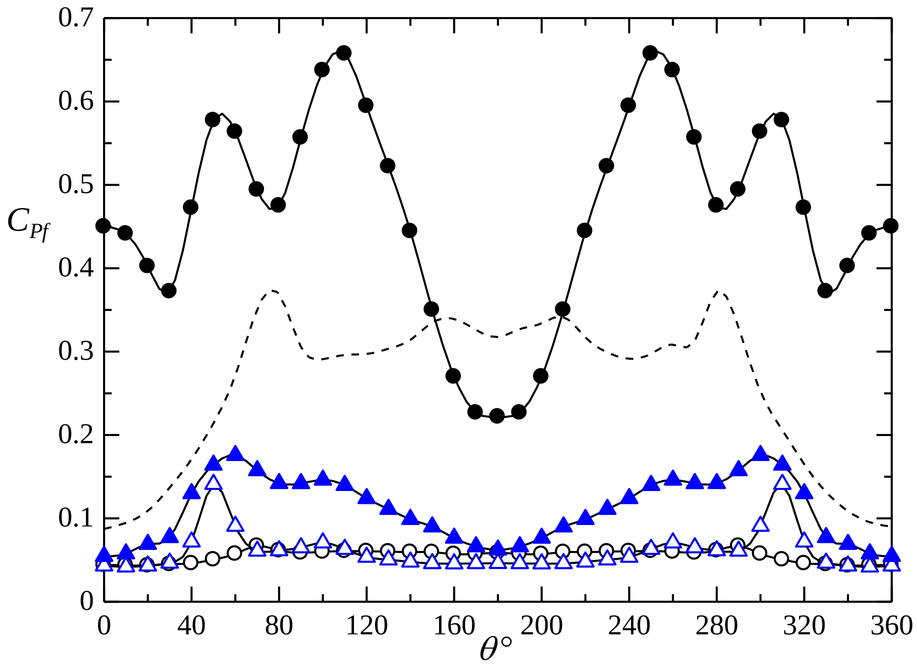

Fig. 8 Fluctuating (rms) pressure coefficient distributions on the surface of the cylinder at $\alpha = 0°$, P^* = 1.4. Plain cylinders: ○, upstream cylinder; ●, downstream cylinder. Tripped cylinders: △, upstream cylinder; ▲ downstream cylinder. - - - -, single plain cylinder.

5.4. Fluctuating pressure on the cylinder surface

Figure 8 displays C_{Pf} measured for the upstream and downstream cylinders at α = 0°, P^* = 1.4 lying in the shear-layer/wake and cylinder interaction regime (Fig. 3). The circular and triangular symbols represent the plain and tripped cylinders, respectively. For the case of the plain cylinders, due to the interaction between the upstream-cylinder shear layer and the downstream cylinder, C_{Pf} over the whole surface of the downstream cylinder is very large, while that on the upstream cylinder is very small as the downstream cylinder acts as a wake stabilizer of the upstream cylinder. On the other hand, for the tripped cylinders, the upstream cylinder C_{Pf} is comparable to that for the plain cylinder, except two peaks at $\theta \approx$ 50° and 310° caused by the shear layer reattachment behind the tripwires as observed for the single tripped cylinder (Fig. 2). That of the downstream cylinder is slightly higher, yet insignificant compared to that of the single plain cylinder or plain downstream cylinder.

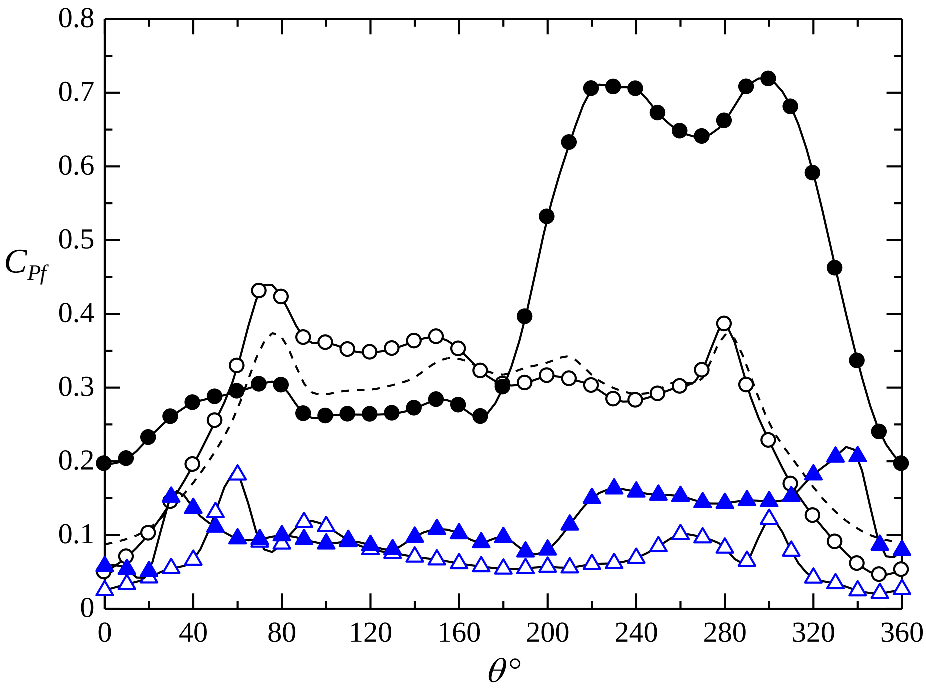

Fig. 9 Fluctuating (rms) pressure coefficient distributions on the surface of the cylinder at α = 25°, P^* = 2.6. Plain cylinders: ○, upstream cylinder; ●, downstream cylinder. Tripped cylinders: △, upstream cylinder; ▲ downstream cylinder. - - - -, single plain cylinder.

Figure 9 shows C_{Pf} measured for the upstream and downstream cylinders at α = 25°, P^* = 2.6 where C_{Lf} on the plain downstream cylinder is the largest (i.e, vortex and shear layer interaction). For the plain cylinders, while C_{Pf} distributions of the upstream cylinder resembles that of the single cylinder, C_{Pf} is very large on the lower surface ($\theta \approx$ 200°- 320°) of the downstream cylinder, due to the incoming vortices from the upstream cylinder (Lee & Smith, 1991; Rockwell, 1998). The flow structure corresponds to that presented in Fig. 6(c). For the tripped cylinders, the upstream cylinder undergoes very small magnitude of C_{Pf}, having very similar C_{Pf} distribution to that for single tripped cylinder (Fig. 2b). C_{Pf} on the downstream cylinder is also small. A slightly increased C_{Pf} at $\theta \approx$ 200°- 330° for the tripped downstream cylinder is due to the upstream cylinder wake disturbance. The observation suggests that the tripped wires have effectively suppressed alternating sheddings from both cylinders. At α = 10°, P^* = 2.6 where C_{Df} is the largest for the plain cylinders, C_{Pf} distributions (not shown) revealed that a large fluctuation in pressure occurring on the front surface of the downstream cylinder results in the large magnitude of C_{Df}. The large fluctuation in pressure suppressed for the tripped cylinders.

6. CONCLUSIONS

An investigation is conducted on the flow interference between two tripped identical cylinders at α = 0° ~ 180° and P^* = 0.1 ~ 5. Two tripwires, each of diameter 0.1D, were attached on each cylinder at azimuthal angle β = ±30°. C_D, C_{Df} and C_{Lf} on the tripped cylinders were measured and compared with those on the plain cylinders at Re = 5.5×10^4. Pressure measurements on the surface of the cylinder were also carried out.

C_D, C_{Df} and C_{Lf} of the plain cylinders are strong function of α and P^*, connected to interaction between boundary layer and cylinder, shear-layer/wake and cylinder, shear layer and shear layer, vortex and cylinder, vortex and shear layer, and vortex and vortex. C_D, C_{Df} and C_{Lf} are very large for the interactions where vortex is involved (i.e., vortex and cylinder, vortex and shear layer, and vortex and vortex). The addition of tripwires suppresses the vortex sheddings from the cylinders, resulting in the suppression of the interactions involving vortex. The large magnitudes of C_D, C_{Df} and C_{Lf} thus reduce to very small values. While the plain cylinders intervene each other extensively, the tripped cylinders do not; hence C_D, C_{Df} and C_{Lf} of the tripped cylinders are almost insensitive to P^* and α. Compared to the plain cylinders, the tripped cylinders experience smaller forces in the entire P^* and α ranges examined. While in most of the region the suppressions in C_D, C_{Df} and C_{Lf} are about 58%, 65% and 85%, respectively, maximum suppressions are 60%, 80% and 90%, respectively.

For the case of the plain cylinders, vortex and shear layer interaction and vortex and cylinder interaction result in a large C_{Pf} respectively on the lower side and front surface of the downstream cylinder. C_{Pf} distribution of the upstream cylinder is comparable to that of a single cylinder. The shear-layer/wake and cylinder interaction brings about a small C_{Pf} on the upstream cylinder and a high C_{Pf} on the downstream cylinder. On the other hand, both tripped cylinders for the all interactions undergo very small C_{Pf} over the whole surface.

ACKNOWLEDGEMENTS

Alam wishes to acknowledge supports given to him from the Research Grant Council of Shenzhen Government through grant KQCX2014052114423867.

REFERENCES

Alam, M. M., Zhou, Y., Zhao, J.M. Flamand, O. and Buojard, O. (2010), “Classification of the tripped cylinder wake and bi-stable phenomenon.” *Int. J. Heat Fluid Flow*, Vol. **31**, 545-560.

Alam, M.M. and Meyer, J.P. (2011), “Two interacting cylinders in cross flow.” *Physical Review E*, Vol. **84**, 056304-16.

Alam, M.M., Moriya, M. and Sakamoto, H. (2003b), “Aerodynamic characteristics of two side-by-side circular cylinders and application of wavelet analysis on the switching phenomenon.” *J. Fluids Struct*., Vol. **18**, 325–346.

Alam, M.M., Sakamoto, H. and Moriya, M. (2003a), “Reduction of fluid forces acting on a single circular cylinder and two circular cylinders by using tripping rods.” *J. Fluids Struct*., Vol. **18**, 347-366.

Alam, M.M. and Sakamoto, H. (2005), “Investigation of Strouhal frequencies of two staggered bluff bodies and detection of multistable flow by wavelets.” *J. Fluids Struct*., Vol. **20**, 425–449.

Alam, M.M., Sakamoto, H. and Zhou, Y. (2005), “Determination of flow configurations and fluid forces acting on two staggered circular cylinders of equal diameter in cross-flow.” *J. Fluids Struct*., Vol. **21**, 363–394.

Aydin, T.B., Joshi, A. and Ekmekci, A. (2014), “Critical effects of a spanwise surface wire on the flow past a circular cylinder and the significance of the wire size and Reynolds number.” *J. Fluids Struct*., Vol. **51**, 132-147.

Blevins, R.D. (1990), *Flow-Induced Vibration, 2nd Edition*. Van Nostrand Reinhold, New York, USA.

Chen, S.S. (1987), *Flow-Induced vibration of circular cylindrical structures*. Washington: Hemisphere Publishing.

Gu, Z.F., Sun, T.F., He, D.X. and Zhang, L.L. (1993), "Two circular cylinders in high-turbulence flow at supercritical Reynolds number." *J. Wind Eng. Indust. Aerodyn.*, Vol. **49**, 379–388.

Igarashi, T. (1981), "Characteristics of the flow around two circular cylinders arranged in tandem (1st report)." *Bull. JSME*, Vol. **24**, 323–331.

James, D.F. and Truong, Q.S. (1972), "Wind load on cylinder with spanwise protrusion." *Proc. ASCE, J. Engng Mech. Div.*, Vol. **98**, 1573-1589.

Kiya, M., Arie, M, Tamura, H. and Mori, H. (1980), "Vortex shedding from two circular cylinders in staggered arrangement." *ASME J. Fluids Eng.*, Vol. **102**, 166–173.

Lee, D. J. and Smith, C. A. (1991), "Effect of vortex core distortion on blade-vortex interaction." *AIAA Journal*, Vol. *29*, 1355-1363.

Medeiros, E.B. and Zdravkovich, M.M. (1992), "Interference-induced oscillation of two unequal cylinders." *J. Wind Eng. Indust. Aerodyn.*, Vol. **41–44**, 753–762.

Nebres, J. and Batill, S. (1993), "Flow about a circular cylinder with a single large-scale surface perturbation." *Exp. Fluids*, Vol. **15**, 369-379.

Paıdoussis, M. P. (1981), "Fluidelastic vibration of cylinder arrays in axial and cross-flow: state of the art." *J. Sound Vib.*, Vol. **76**, 329-360.

Paıdoussis, M. P. (1993), "Some curiosity-driven research in fluid structure interactions and its current applications. Calvin Rice lecture." *ASME J. Press. Vessel Tech.*, Vol. **115**, 2-14.

Price, S.J. and Paıdoussis, M.P. (1984), "The aerodynamic forces acting on groups of two and three circular cylinders when subject to a cross-flow." *J. Wind Eng. Indust. Aerodyn.*, Vol. **17**, 329–347.

Rockwell, D. (1998), "Vortex-body interactions." *Ann. Rev. Fluid Mech*., Vol. **30**, 199-229.

Sakamoto, H., Haniu, H., Obata. Y. and Matubara, S. (1994), "Optimum suppression of fluid forces acting on a circular cylinder and its effectiveness," *JSME Int. J.*, Series B, Vol. **37**(2), 369-376.

Sumner, D., Price, S.J. and Paidoussis, M.P. (2000), "Flow-pattern identification for two staggered circular cylinders in cross-flow." *J. Fluid Mech.*, Vol. **411**, 263–303.

Sun, T.F., Gu, Z.F., He, D.X. and Zhang, L.L. (1992), "Fluctuating pressure on two circular cylinders at high Reynolds numbers." *J. Wind Eng. Indust. Aerodyn.*Vol. **41–44**, 577–588.

Szepessy, S. and Bearman, P.W. (1992), "Aspect ratio and end plate effects on vortex shedding from a circular cylinder." *J. Fluid Mech.*, Vol. **234**, 191-217.

West, B.G. and Apelt, C.J. (1982), "The effect of tunnel blockage and aspect ratio on the mean flow past a circular cylinder with Reynolds number between 10^4 and 10^5." *J. Fluid Mech.*, Vol. **114**, 361-377.

West, G.S. and Apelt, C.J. (1993), "Measurements of fluctuating pressures and forces on a circular Cylinder in the Reynolds number range 10^4 to 2.5×10^5." *J. Fluids Struct.*, Vol. **7**, 227-244.

Zdravkovich, M.M. (1988), "Review of interference-induced oscillations in flow past two parallel circular cylinders in various arrangements." *J. Wind Eng. Indust. Aerodyn.* Vol. **28**, 183-200.